PAPER • OPEN ACCESS

Bending and reverse bending during the fabrication of novel GaAs/(In,Ga)As/GaAs core–shell nanowires monitored by *in situ* x-ray diffraction

View the article online for updates and enhancements.

Bending and reverse bending during the fabrication of novel GaAs/(In,Ga)As/GaAs core–shell nanowires monitored by *in situ* x-ray diffraction

Ali Al Hassan[1] , Mahmoud AlHumaidi[1,2], Jochen Kalt[1,2],
Reinhard Schneider[3], Erich Müller[3], Taseer Anjum[4], Azat Khadiev[5],
Dmitri V Novikov[5], Ullrich Pietsch[4] and Tilo Baumbach[1,2]

[1] Institute for Photon Science and Synchrotron Radiation, Karlsruhe Institute of Technology, Hermann-von Helmholtz-Platz 1, D-76344 Eggenstein-Leopoldshafen, Germany
[2] Laboratory for Applications of Synchrotron Radiation, Karlsruhe Institute of Technology, Kaiserstraße 12, D-76131 Karlsruhe, Germany
[3] Laboratory for Electron Microscopy, Karlsruhe Institute for Technology, D-76128 Karlsruhe, Germany
[4] Solid State Physics, University of Siegen, Walter-Flex Straße 3, D-57068, Siegen, Germany
[5] DESY Photon Science, Notkestr. 85, D-22607 Hamburg, Germany

E-mail: ali_al_hassan@live.com

Abstract

We report on the fabrication of a novel design of GaAs/(In,Ga)As/GaAs radial nanowire heterostructures on a Si 111 substrate, where, for the first time, the growth of inhomogeneous shells on a lattice mismatched core results in straight nanowires instead of bent. Nanowire bending caused by axial tensile strain induced by the (In,Ga)As shell on the GaAs core is reversed by axial compressive strain caused by the GaAs outer shell on the (In,Ga)As shell. Progressive nanowire bending and reverse bending in addition to the axial strain evolution during the two processes are accessed by *in situ* by x-ray diffraction. The diameter of the core, thicknesses of the shells, as well as the indium concentration and distribution within the (In,Ga) As quantum well are revealed by 2D energy dispersive x-ray spectroscopy using a transmission electron microscope. Shell(s) growth on one side of the core without substrate rotation results in planar-like radial heterostructures in the form of free standing straight nanowires.

Keywords: *in situ* x-ray diffraction, bending and reverse bending, radial nanowire heterostructures, energy dispersive x-ray spectroscopy, molecular beam epitaxy

Introduction

The monolithic growth of GaAs nanowires on the mature Si platform presents new potentials for a wide range of future applications in nanotechnology [1–4] due to its high carrier mobility, and direct band gap which is suitable for single-junction solar cells. The large lattice mismatch (∼4.1%) and difference in their thermal expansion coefficients (∼60%) complicates planar GaAs growth on Si substrates [5, 6]. However, GaAs nanowires can be grown on Si substrates without the formation of extended defects [7], where the misfit strain relaxes either elastically to the surface or plastically via the formation of misfit dislocations which is confined to the reduced interface area [8]. Furthermore, their unique geometry enables the fabrication of core/shell heterostructures of highly lattice-mismatched materials well beyond the limits for coherent growth in equivalent thin-film

heterostructures [9, 10]. The lattice mismatch between the core and shell can be accommodated via elastic deformation of both, depending on the relative thicknesses and chemical compositions [11].

To date, III–V LEDs on Si have been demonstrated using several heterostructure nanowire systems [12–14]. Visible blue light emission is achieved by GaN-based nanowires whereas near-infrared (IR) range emission is provided by GaAs-based nanowires with longest emission wavelength of about 830 nm. However, LEDs operating at the telecommunication wavelengths 1.3 and 1.5 μm for optical fiber technology require the employment of narrow band gap III–V semiconductors as the active medium. A reasonable choice is (In,Ga)As as its band gap could span from the near-IR to the mid-IR range depending on its indium content. On the one hand, the impact of the (In,Ga)As quantum well thickness on the optical properties of GaAs/(In,Ga)As/GaAs core/shell nanowires grown epitaxially on Si have been explored in [15]. By contacting an ensemble of free-standing nanowires, the authors achieved room-temperature emission at 985 nm showing great potential for near-IR light emission on the Si platform. On the other hand, axial strain in GaAs/(In,Ga)As core/shell nanowires has been investigated for different indium concentrations [16]. Above a critical indium content, an anomalous strain relaxation process has been revealed where the (In,Ga)As shell grows simultaneously as a coherent shell and as plastically relaxed mounds. Strain induced by the (In,Ga)As shell onto the GaAs core can be utilized to control and optimize the optical properties of the nanowire. For instance, in a more recent study, it was shown that the bandgap of GaAs nanowires grown epitaxially on Si substrates can be reduced by up to 40% when overgrown with lattice-mismatched (In,Ga)As or (In,Al)As shells [17].

Apart from the constant biaxial strain discussed in the above-mentioned studies of GaAs/(In,Ga)As-based core/shell nanowires, the realization of spatially varying strain fields offered by nanowire bending opens up new possibilities to control the motion of charge carriers [18, 19], and furthermore to form nanowire networks and interconnects [20]. Asymmetric (In,Ga)As shell growth on a lattice-mismatched GaAs core results in asymmetric strain across the nanowire heterostructure, which is sufficient to bend vertical nanowires [21–23]. Photoluminescence spectroscopy performed on bent GaAs/(In,Ga)As core/shell nanowires revealed that varying strain fields induce charge carrier drift toward the tensile-strained part of the nanowires, and that the polarization response of absorbed and emitted light is controlled by the bending direction.

In this work, we cover both scenarios mentioned above; (1) nanowire bending resulting in a spatially varying strain field, and (2) reverse bending up until the nanowires are straight again, which is yet to be reported for the same nanowire system. As a result, we present a novel design of GaAs/(In,Ga)As/GaAs radial heterostructures that are analogous to planar layers but grown in the form of free standing nanowires. First, uncapped straight and strain free GaAs nanowires are grown perpendicular to the surface of the Si 111 substrate. Second, (In,Ga)As shell growth is carried out

without substrate rotation, which results in nanowire bending along a well-defined direction for a Si substrate covered with native oxide [22]. Finally, the GaAs outer shell is deposited on top of the (In,Ga)As shell, resulting in reverse nanowire bending, up until the nanowires are fully straight. Bending and reverse bending are a result of axial strain induced by the deposited shell on the preceding layer, which will be explained in more details later. In turn, axial strain can be controlled by either the core to shell(s) volume ratio, or indium content of the quantum well. However, for this particular study, we keep the (In,Ga)As alloy composition constant, and inspect bending, reverse bending and axial strain during the growth process of both shells.

Owing to its spatial atomic resolution, a transmission electron microscope (TEM) stands out as the principle device in monitoring layer-by-layer growth of single crystalline nanowires [24, 25]. However, despite the paramount importance of such experiments in understanding growth dynamics, investigating nanowire bending *in situ* by TEM is extremely challenging, and the reasons are manifold, including (1) restricted sampling area and thickness, making it complicated to measure more than one nanowire from the same sample during the bending process, (2) the unpredictability of the nanowire bending direction, (3) controlled shell growth on only one side of the core in TEM is yet to be established, and (4) nanowires grown on substrates covered with native oxide possess slightly different structural properties i.e. core diameter, nanowire length, and shell composition and thickness, which leads to slightly different bending comparing individual nanowires. Therefore, in this case, statistical data based on ensemble measurement is more meaningful than single ones. However, complementary TEM performed after nanowire bending or straightening can still provide very valuable information i.e. shell composition and thickness.

Alternatively, *In situ* diffraction using high brilliance monochromatic x-rays at synchrotron radiation facilities serves as an ideal technique to investigate strain and the bending evolution [22, 23] of nanowires due to its high sensitivity to atomic displacement in the angstrom range [16, 26], and changes in the lattice orientation that are not even visible by a scanning electron microscope [27]. Moreover, XRD provides information about bending in 3D real space, and can be performed on nanowire ensembles for meaningful statistical study since nanowires grown on a common substrate exhibit slightly different structural properties due to different local growth conditions such as competition for growth species by neighboring nanowires [28]. In this work, we visualize progressive bending and reverse bending, and calculate the variation in the axial strain based on the 111 Bragg reflection which is recorded during the MBE growth of the (In,Ga)As quantum well and GaAs outer shell.

Sample preparation and growth

The Si substrate went through regular solvent cleaning steps consisting of two rounds of subsequent dipping into acetone,

isopropanol and ultra-pure water baths in an ultrasonic cleaner before being loaded into our portable MBE (pMBE) chamber designed for *in situ* diffraction experiments on III–V nanowires [29]. The substrates were then degassed in a loadlock at 300 °C for 30 min to dissolve the solvent residuals and water.

The growth of the nanowires was conducted in a three-step process following [30]. First, the substrate was annealed in the MBE reactor at a temperature of approximately 730 °C for 30 min. In the second step, 16 monolayers (ML) of Ga (given as an equivalent of planar GaAs(001) growth here and in the following) are deposited to form liquid droplets on the native oxide of the Si(111) surface at substrate temperature, $T_{sub} = 570$ °C in order to etch nanosized holes into the SiO_x layer. These droplets are then desorbed from the surface by annealing the substrate surface again at 730 °C. In the third step, an equivalent of 8 ML of Ga is deposited at 610 °C to form droplets in the pre-etched holes. After droplet formation, the nanowires are grown in VLS mode by simultaneous supply of Ga and As for 30 min with equivalent rates of $0.08 \, ML \, s^{-1}$ and $0.24 \, ML \, s^{-1}$, respectively. The nominal nanowire length is around 0.8–1 μm for the *in situ* investigated sample, and around 1.8–2 μm for the *ex situ* grown samples.

Afterwards, the substrate is cooled down to approximately 400 °C and the (In,Ga)As shell was deposited for 10 min, and then 5 min (total growth time = 15 min) at only one side of the GaAs nanowires without substrate rotation. The equivalent fluxes were $0.05 \, ML \, s^{-1}$ for Ga, $0.004 \, ML \, s^{-1}$ for In and $0.28 \, ML \, s^{-1}$ for As, i.e. an In/Ga ratio of about 8%. The sample was then rotated by 120° in order to deposit the outer GaAs shell on top of the (In,Ga)As shell. After rotation, the GaAs outer shell was deposited in six steps of 10 min and one with 20 min (total growth time = 80 min) using the same Ga and As fluxes as for the (In,Ga)As shell. The objective behind intermittent shell growth is to record the nanowire Bragg reflection after each deposition step enabling the inspection of nanowire bending and subsequent straightening as a function of growth time.

GaAs nanowires usually adapt the ZB crystal structure with the presence of short WZ segments at the nanowire bottom due to the small size of the droplet at the beginning of the growth, and at the nanowire top section due to As consumption which precedes radial shell growth [27, 31]. However, the WZ Bragg reflection is not visible in later XRD reciprocal space maps, and therefore the nanowire crystal structure is considered to be pure ZB. The (In,Ga)As and GaAs shells adapt the crystal structure of the core.

Experimental details

In order to inspect the axial strain evolution *in situ*, i.e. during nanowire bending and reverse bending, diffraction has to be conducted inside the growth chamber. To accomplish this, first, our pMBE chamber was transported to the *in situ* and Nano x-ray diffraction beamline P23 at PETRA III one week prior to the XRD experiment. During this week we setup the system and perform functionality tests i.e. calibration of the growth rate and optimization of nanowire growth, which is crucial for the success of the XRD experiment. Second, in order to initiate the diffraction measurements, we ensemble the pMBE, which is equipped with couple of beryllium windows through which x-rays can enter and exit, on the heavy load diffractometer available at the beamline. The x-ray beam was focused to a size of 2 μm (v) × 5 μm (h) at photon energy of 15 keV by means of hexapod-mounted compound-refractive lens focusing setup. To investigate the axial strain evolution during nanowire bending, we recorded the 3D distribution of the scattered x-ray intensity in the vicinities of the symmetric Si and GaAs 111 Bragg reflections using a 2D LAMBDA pixel detector (512 pixels (v) × 1536 pixels (h)) with a time resolution up to 2 kHz. At 15 keV, the Bragg condition with the GaAs 111 lattice planes is fulfilled at incident and exit angles of 7.27° and 14.54°, and with Si 111 at 7.57° and 15.14°. At sample-to-detector distance of about 1 meter and pixel size of 55 μm, the LAMBDA detector covers an angular range of 1.6° vertically, which is larger than the difference in the scattering angles of both reflections. Therefore, to record 3D intensity maps of both reflections, one needs to perform incident angle scans around the Bragg angles of GaAs and Si 111 at a fixed detector angle. The 3D intensity distribution can then be plotted as a function of the horizontal and vertical angular ranges covered by the detector, and the incident angle. The angular coordinate system is then translated to reciprocal space vectors Q_x, Q_y and Q_z following [32], to create the so-called 3D reciprocal space map (RSM). Q_z is defined along the nanowire growth axis (figure 1) and is sensitive to changes in the axial lattice spacing, whereas Q_x and Q_y are defined perpendicular to Q_z and are sensitive to changes in the lattice orientation i.e. tilting or bending. Finally, Q_B defines the bending direction of the nanowires in reciprocal space.

SEM results

The most commonly used technique to visualize nanowire bending in real space is scanning electron microscopy (SEM). However, SEM requires removing the sample from the MBE chamber, which makes it impossible to monitor progressive nanowire bending and reverse bending *in situ* during shell(s) growth. Nonetheless, the nanowire growth procedure used for the *in situ* experiment, can be replicated *ex situ* on different Si 111 wafers using identical growth conditions. Figure 1 shows top view SEM micrographs of GaAs/(In,Ga)As/GaAs core/shell nanowires grown on different Si 111 substrates with 10 min (a), 20 min (b), 30 min (c), 40 min (d), 50 min (e), and 60 min (f) of GaAs shell growth time. Figures 1(g), (h) are top and 30° tilt view SEM images taken from the *in situ* measured sample (80 min GaAs shell growth). The nanowire tip and bottom are imaged using different contrasts, as indicated in figure 1(a). Looking at the nanowires from top (figures 1(a)–(g)), the tip and bottom would overlap if the nanowires are straight and perpendicular to the substrate surface (see figure 1(g)), whereas they would be distinguishable if the
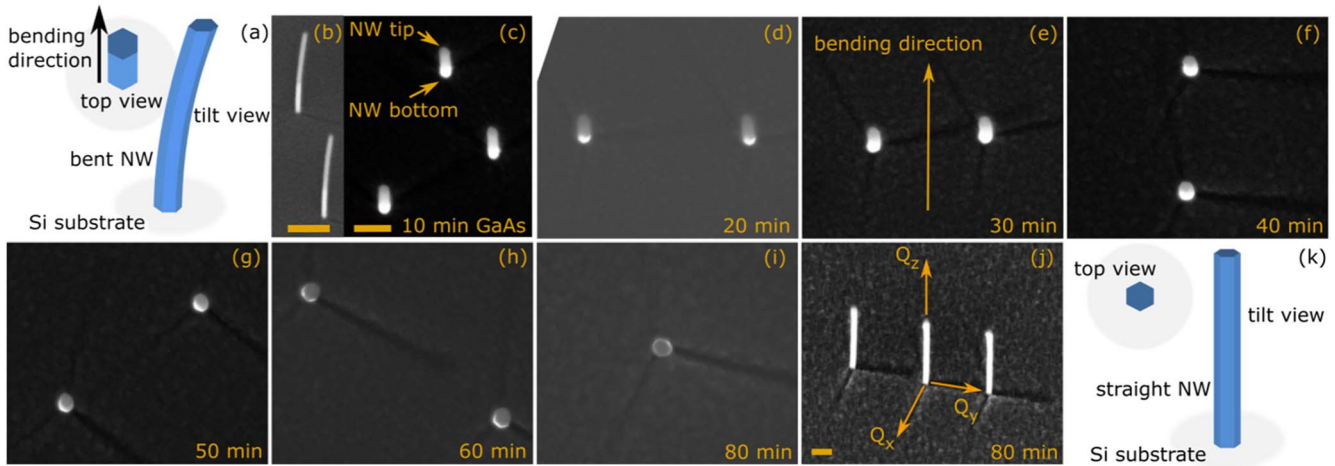
Figure 1. Animations of bent and straight nanowires in tilt and top views are shown in panels (a) and (k), respectively. (b) 30° tilt view SEM image of GaAs/15 min (In,Ga)As/ 10 min GaAs nanowires taken perpendicular to the bending direction. (c)–(j) Top view SEM micrographs of GaAs/(In,Ga)As/GaAs nanowires with 10, 20, 30, 40, 50, 60 and 80 min of GaAs outer shell growth time. (j) 30° tilt view SEM micrograph of nanowires with 80 min GaAs outer shell growth time. The scale bar in (c) scales to 200 nm, and applies to panels (c)–(j). The scale bars in (b) and (j) scale to 500 nm and 100 nm respectively.

nanowire is bent (see figure 1(a)). It is evident that as the growth time of the GaAs outer shell increases, the nanowire tip and the bottom come closer, meaning that nanowire bending is being reversed. As demonstrated in figures 1(g), (h), after 80 min of GaAs shell growth, the nanowires are completely straight and perpendicular to the substrate surface.

XRD results

When the nanowires are perfectly parallel to the substrate normal, the x-rays diffracted from the 111 lattice planes will coincide at $Q_x = Q_y = 0$ in reciprocal space. Therefore, tilting of the whole nanowire is resembled by a shift of the total Bragg reflection along the (Q_x,Q_y) plane i.e. the larger the tilting is in real space the larger the shift is from $Q_x = Q_y = 0$ in reciprocal space. On the other hand, nanowire bending, and thereby continuous tilting of the lattice planes, is featured by elongation of the Bragg reflection along the Debye–Scherrer ring due to the continuous angular change of the lattice planes. This is accompanied by peak broadening along the strain sensitive direction, Q_z, due to a gradient in the lattice spacing across the nanowire diameter. For sake of simplicity and clarity, only 2D RSMs extracted along the bending direction, Q_B, and projections along the (Q_x, Q_y) plane will be presented in the following. Additionally, the Si substrate being unstrained, its Bragg reflection is utilized as reference to calculate the absolute axial strain in the nanowire. However, the Si peak provides no other significance, and therefore will be omitted from the 2D RSMs, where only the nanowire Bragg peak will be presented.

To envision nanowire tilting and bending away from the substrate normal in real space, we project the 3D intensity distribution of the 111 Bragg reflection along the (Q_x, Q_y) plane in reciprocal space after growth of the GaAs core and every shell deposition step. The RSMs are stacked on top of

each other in figure 2 in order to directly visualize the nanowire bending evolution comparing consecutive growth steps. The yellow circle located at $Q_x = Q_y = 0$ denotes the position of the Si crystal truncation rod (CTR) which represents our reference to calculate any change in the orientation of the nanowire 111 lattice planes. The Bragg reflection of the GaAs cores (figure 2(a)) being slightly shifted from the Si CTR but symmetric in shape translates to the nanowires being slightly tilted with respect to the substrate normal but straight. Extracting Q_B and Q_z from the center of the Bragg reflection, the mean initial tilt of the measured nanowire ensemble is calculated to be 0.03° using $\tan^{-1}(|Q_B/Q_z|)$, demonstrating the high sensitivity of XRD in detecting changes in the nanowire orientation. After 10 and 15 min of (In,Ga)As shell growth onto one side of the GaAs cores, the signal elongates along Q_B (figures 2(b), (c), which can be explained by continuous tilting of the 111 lattice planes (in other words, nanowire bending) along a defined direction. In a recent study, it was shown that at this substrate temperature, the (In, Ga)As shell grows at the side facets facing the As flux [22]. Therefore, to ensure the deposition of the GaAs outer shell onto the (In,Ga)As shell, the sample was rotated by 120° which is the angular separation between the Ga and As effusion cells inside the pMBE With increasing the thickness of the outer GaAs shell (figures 2(d)–(j)), the nanowire Bragg reflection gradually retracts towards the Si CTR, which implies that the nanowires are straightening, and accordingly the nanowire 111 lattice planes are aligning back parallel to the substrate surface. However, comparing the first (figure 2(a)) and last (figure 2(j)) RSMs, it is evident that the diffraction signal does not shift back to its exact original position prior to (In,Ga)As shell growth. This suggests that the nanowire bending caused by (In,Ga)As shell growth was preceded by slight tilting which could not be recovered.

To monitor the axial strain evolution during nanowire bending and reverse bending, we extract 2D cuts from the 3D
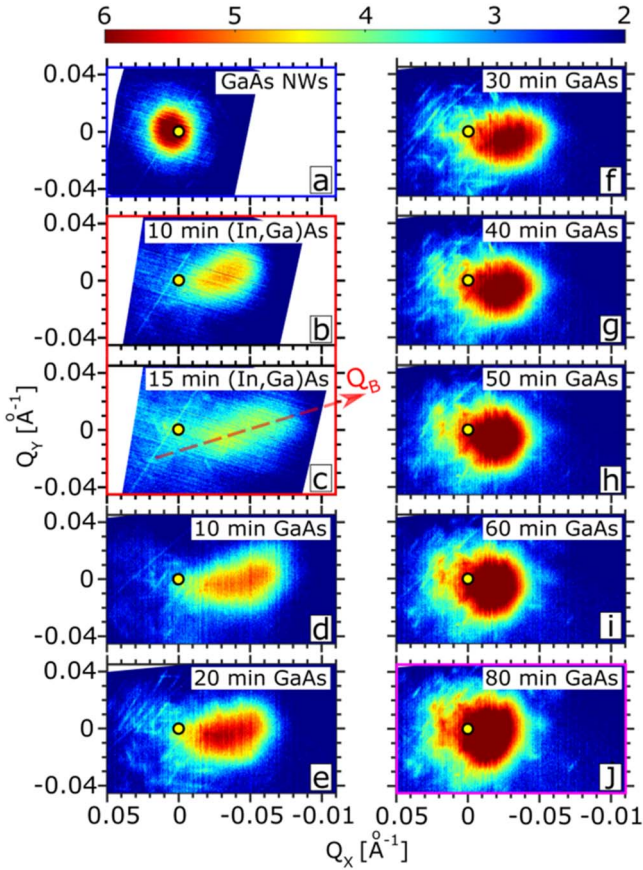
Figure 2. Intensity distribution of the 3D 111 Bragg reflection projected into the (Q_y, Q_x) plane in reciprocal space. The bending direction in reciprocal space, Q_B, is indicated by a red arrow in subplot (c). The RSMs are recorded for bare GaAs cores (a), then after 10 min (b) and 15 min (c) of (In,Ga)As shell growth time, followed by 10 min (d), 20 min (e), 30 min (f), 40 min (g), 50 min (h), 60 min (i), and 80 min (j) of GaAs outer shell growth time. For better traceability, the shell growth time and material are listed at the top left corner of each RSM. The frame of each RSM is colored in accordance to its corresponding atomic animation in figure 3(c).

Bragg reflection along the bending plane, (Q_B, Q_z), in reciprocal space after core growth and every shell deposition step. Analogous to figure 2, the 2D maps are stacked on top of each other in figure 3(a), where the respective growth material and time are listed at the top left corner of each map. The animations displayed in figure 3(b) correspond to the nanowire cross-section expected after each growth step in figure 3(a). To explain the induction of nanowire bending and reverse bending during different stages of (In,Ga)As and GaAs shell growth, the variation in the 111 lattice spacing of both materials is portrayed in the atomic animation of figure 3(c) i.e. GaAs atoms are colored in blue whereas the (In,Ga)As lattice is colored in red. Each atomic animation in figure 3(c) and its corresponding RSM(s) in figure 3(a) are framed using the same color, i.e. blue for the unstrained bare GaAs core, red for the bent nanowires after (In,Ga)As shell growth, and green for the nanowires after the growth of the GaAs outer shell. The 111 Bragg reflection measured after the growth of the GaAs cores is depicted at the top of figure 3(a). The signal being symmetrically centered at the Si CTR suggests that the

nanowires are perfectly parallel to the substrate normal. After 10 and 15 min of (In,Ga)As shell growth on one side of the GaAs nanowire cores, the diffracted signal changes. On the one hand, the signal elongates in Q_B along the Debye–Scherrer ring, indicating nanowire bending due to strain induced by the shell onto one side of the core. On the other hand, the Bragg reflection shifts towards lower Q_z values. This indicates that the axial expansion of the GaAs core and the compression of the (In,Ga)As shell results in a shared lattice spacing that is larger than that of unstrained GaAs ($Q_z = 1.925\,\text{Å}^{-1}$). Longer (In,Ga)As growth time translates to a larger (In,Ga)As/GaAs volume ratio. This induces a larger axial tensile strain on the GaAs core, and strain relaxation of the (In,Ga)As shell resulting in a larger shift of the signal towards lower Q_z. The tensile and compressive strains of the core and shell at the hetero-interface are faced by opposite strains at their surfaces, which leads to nanowire bending and an axial strain gradient across the nanowire diameter. After rotating the substrate by 120° around its normal, the GaAs outer shell was grown on top of the (In,Ga)As shell in six steps of 10 min and a final step of 20 min, which translates to a total growth time of 80 min. It is evident from the first to the last growth step that the signal (1) retracts along the Debye–Scherrer ring towards the Si CTR implying that the nanowires are straightening, and (2) shifts towards higher Q_z values as the deposition time increases, denoting a decrease in the shared axial lattice spacing. This indicates a larger compressive strain on the (In,Ga)As shell at the hetero-interfaces, faced by strain relaxation of the GaAs core and outer shell. As displayed in the atomic animation framed in green, the GaAs outer shell exerts compressive strain on the (In,Ga)As lattice at the interface faced by expansion at the surface of the GaAs core, resulting in reverse nanowire bending. Progressive GaAs shell growth leads to larger reverse bending until the nanowire is fully straightened, as illustrated by the atomic animation framed in magenta color.

To quantify the mean axial strain in the measured nanowire ensemble as a function of shell growth time (see figure 3(d)), we first extract line profiles perpendicular to the center of the Bragg reflection in Q_B, which corresponds to the nanowire midsection in real space. Second, the line profiles are fitted by Gaussian functions, and the peak position of the strained lattice, $Q_{z,f}$, is plugged into

$$\varepsilon_{zz} = (Q_{z,f} - Q_{z,i})/Q_{z,i},$$

where $Q_{z,i}$ is the position of unstrained GaAs along the scattering direction in reciprocal space, and ε_{zz} denotes axial strain. In addition, the axial strain gradient calculated from the FWHM of the Bragg peak in Q_z is displayed in figure 3(d) in the form of olive color shade. The bare GaAs cores (prior to shell growth) are considered unstrained ($\varepsilon_{zz} = 0$, green data point), and the corresponding FWHM of the peak is considered as a reference for zero strain gradient. As expected, during (In,Ga)As shell growth (see red colored data points) the core undergoes tensile strain, reaching a value of 0.08% after 15 min of growth. As illustrated by the blue colored data points, during growth of the GaAs outer shell, the mean axial strain and its gradient decrease exponentially. After 70 min of
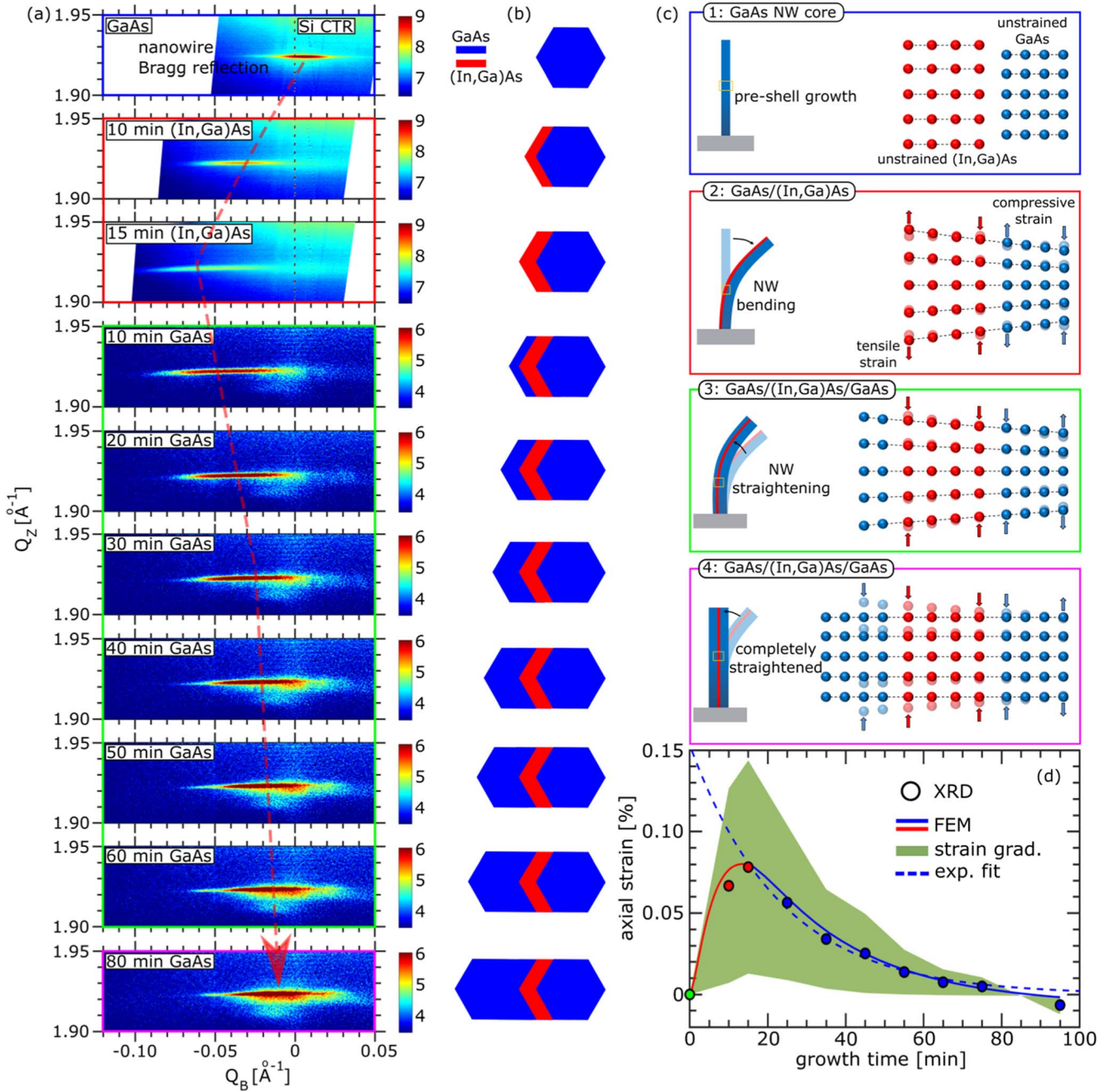
Figure 3. (a) 2D RSMs extracted along the nanowire bending direction, Q_{B}, in reciprocal space. The shell growth time and material are listed at the top left corner of each RSM. The shift of the peak center in Q_{B} is indicated by a red arrow. (b) The core/shell nanowire cross-sections expected after each growth stage in (a). (c) Atomic animations to demonstrate the variation in the axial lattice spacing of the core and shells prior to (1) and during the deposition of the (In,Ga)As (2) and GaAs shells (3)–(4). The transparent atoms correspond to the lattices from the previous step, and the arrow direction indicates if the strain is tensile or compressive. (d) Axial strain as a function of shell growth time. The green data point corresponds to zero strain for bare GaAs nanowires, whereas the blue and red data points represent values of axial strain during (In,Ga)As and GaAs shell growth respectively.

GaAs shell growth (total growth time = 85 min in figure 4(c)), the nanowire fully recovers its axial lattice parameter pre-shell deposition (zero strain, similar to the green data point) with no strain gradient. The fact that there is zero strain but the Bragg peak does not fully recover its (Q_x, Q_y) position pre-shell deposition (see figure 2) confirms that the nanowires are fully straightened, meaning that the

111 lattice planes are parallel to each other, but still slightly tilted with respect to the substrate normal. This strengthens our assumption that the nanowires have tilted slightly before bending which is possible to occur at the beginning of (In,Ga) As shell growth. The axial strain evolution follows an exponential function where the shared axial lattice parameter of the core and shell is expected to match that of unstrained GaAs
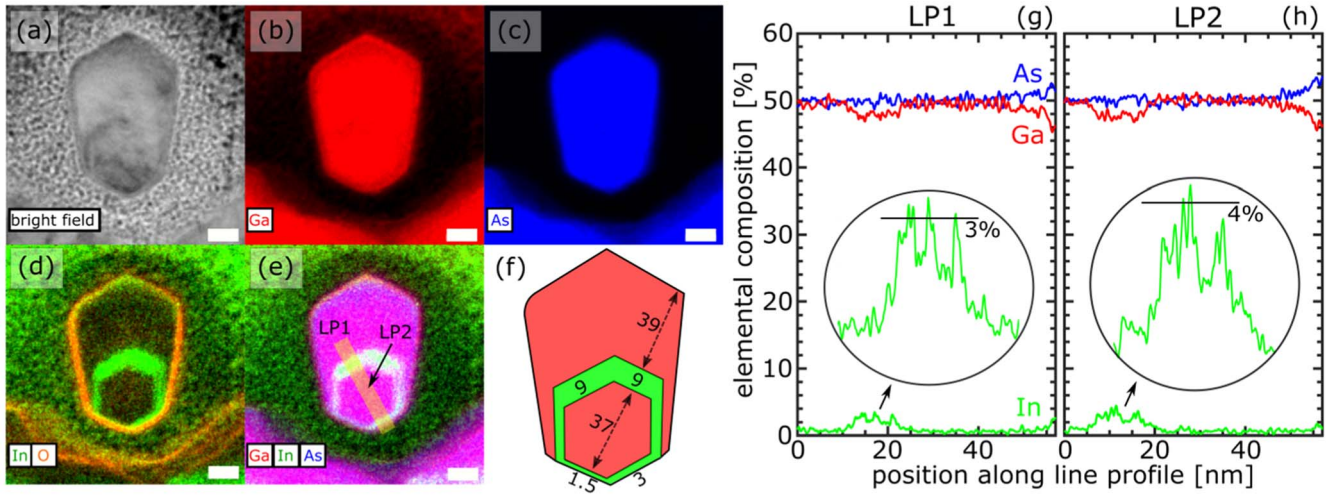
Figure 4. (a) HAADF micrograph of the nanowire cross-section surrounded by Pt protective layer. EDX 2D maps of the nanowire elemental composition colored in red for Ga (b), blue for As (c), and green for In + orange for O (d). The EDX maps of Ga, In and As are superimposed in (e) i.e. GaAs and (In,Ga)As are represented in pink and light green respectively. The diameter of the GaAs core, and thicknesses of the (In,Ga)As quantum well and the GaAs outer shell are displayed in (f). (g) and (h) show line profiles LP1 and LP2 extracted from the EDX map in (e), and are indicated by transparent yellow box and black arrow, respectively.

for large GaAs/(In,Ga)As volume ratio, and not to compress more during further GaAs shell deposition.

FEM results

For a better understanding of nanowire bending and reverse bending at different stages of shell(s) growth, we employed and solved the analytical model presented in [21] using the finite element method (FEM). The analytical model provides the axial strain distribution within the nanowire as a function of the stressor shell(s) growth time. First, a hexagonal nanowire cross-section, a core diameter estimated from TEM to be 37 nm (see later), and an (In,Ga)As shell with 8% nominal indium composition approximated from growth and EDX were implemented into the model as input. Second, to initiate the FEM simulations, the growth rates of the (In,Ga)As and GaAs shells are approximated from the final thicknesses estimated by TEM (see later) and growth times. The shells were then varied in thicknesses until the experimental axial strain values in figure 3(d) were matched. It is important to mention that our simplified FEM model disregards all-around shell growth, and instead considers an asymmetric (In,Ga)As shell grown on only one side of the GaAs core. The (In,Ga)As shell is then overlaid by an asymmetric GaAs outer shell.

Conventional fixed-free boundary conditions from the Euler–Bernoulli beam theory are applied at the opposite side-walls of the core and shells. Since geometrical nonlinearities are not considered, the generalized Hooke's law can be used to express the relation between stress and strain in a continuous elastic material as [33, 34]

$$\sigma_{ij} = C_{ijkl}\ \epsilon_{kl} \ \text{ or } \ \epsilon_{ij} = S_{ijkl}\ \sigma_{kl}$$

where C_{ijkl} and S_{ijkl} are defined as the tensors of stiffness and compliance of fourth rank, respectively. Conversely, σ_{ij} and ϵ_{kl} are second rank stress and strain tensors, respectively.

For the FEM simulation, we assume that the core and the shells are pure zinc blende cubic crystals, and in a conventional coordinate system for crystal plane (100) the stiffness coefficient matrix reduces to a matrix with only three independent elastic constants.

$$C_{\text{ZB},ij} = \begin{bmatrix} C_{11} & C_{12} & C_{12} & & & \\ C_{12} & C_{11} & C_{12} & & & \\ C_{12} & C_{12} & C_{11} & & & \\ & & & C_{44} & & \\ & & & & C_{44} & \\ & & & & & C_{44} \end{bmatrix},$$

where the elastic constants for GaAs are $C_{11} = 124.2$ GPa, $C_{12} = 51.4$ GPa, and $C_{44} = 63.4$ Gpa [35]. The elastic constants for the (In,Ga)As shell were obtained by linear interpolation between InAs and GaAs. For 8% In content, the elasticity constants for the (In,Ga)As shell are estimated to be $C_{11} = 116.15$ GPa, $C_{12} = 52.76$ GPa, and $C_{44} = 57.99$ GPa.

The nanowires grow in the [111] direction, and therefore their respective stiffness matrices need to be rotated to align the nanowire's *z*-axis along the [111] crystallographic direction. More information about such matrix transformations has been extensively reported and can be found elsewhere [33, 36].

Given the magnitude of the misfit strain between GaAs and (In,Ga)As within our system is small (nominal indium concentration of about 8%), the two-dimensional FEM simulations are carried out based on the linear elasticity theory, and therefore the inclusion of geometrical nonlinearities is not included. Conventional fixed-free boundary conditions from Euler–Bonoulli beam theory are applied at the opposite side-walls of the core and shells. The estimated lattice mismatch between the core and the asymmetric shells from the analytical model are simulated as initial strain input in the FEM model to extract axial strain at the nanowire midsection

during bending and reverse bending as function stressor shell(s) deposition time. As a result, figure 3(d) shows an excellent agreement between the experimental data and the average strain simulated by FEM.

TEM/EDXS results

To inspect precisely the nanowire morphology and the elemental distribution of In, Ga, and As, we need to look at the nanowire basal plane which exposes the core/shell/shell heterostructure. To achieve this, an individual 2 μm long nanowire from the *in situ* measured sample was milled down to around 70 nm by means of a Ga focused ion beam i.e. the incident beam was perpendicular to the nanowire growth axis. Prior to milling, the nanowire was covered by a protective Pt layer. A TEM bright field micrograph of the resulting nanowire cross-section is displayed in figure 4(a). Since this method is sensitive to the atomic mass of the species, with In ($Z = 49$) having a higher atomic number than Ga ($Z = 31$), the (In,Ga)As quantum well should appear in darker contrast compared to GaAs. Its morphology, however, is not fully resolved due to its low In content. Qualitative energy dispersive x-ray spectroscopy (EDXS) 2D maps of the Ga, As and In (superimposed with O) distributions are displayed in figures 4(b)–(d) with an acquisition time of 4814 sec per map. Comparing the As and Ga distributions in figures 4(b) and (c) respectively, an additional Ga layer of lower contrast compared to the central nanowire region is found at the nanowire surface. The similar presence of O at the nanowire surface (see figure 4(d)) suggests the formation of a Ga_2O_3 shell during milling. The gallium oxide shell thickness is equivalent to that of O, which measures to 4 nm. Finally, to demonstrate the core/shell/shell nanowire configuration, Ga, In and As are overlapped in figure 4(e). Indeed, the GaAs outer shell, on the one hand, grows only at the (In,Ga)As sidewalls facing the Ga flux inside the MBE. On the other hand, due to its larger diffusion length compared to Ga, In defuses slightly around the GaAs core. For quantitative EDXS analysis of the In concentration and thickness of the (In,Ga)As shell we extract line profiles (LP1 and LP2) across the shell as indicated by a transparent orange rectangle for LP1 in figure 4(e). Line profile LP2 is extracted in a similar fashion to LP1 along the direction defined by a black arrow. The resulting line profiles LP1 and LP2 are shown in figures 4(g) and (h), respectively. The Ga and In percentages in the quantum well are 47% and 3% along LP1, and 46% and 4% along LP2. This means that the In concentration in the shell is around 6%–8% if As is scaled to 100%. This is in good agreement with the In concentration estimated from the growth parameters. The diameter and thicknesses of the core and shells are shown in figure 4(f). The GaAs core diameter is 37 nm, (In,Ga)As shell thickness is 9 nm, and the thickness of the GaAs outer shell measures to 39 nm. This implies that equal strain is exerted on the (In,Ga)As shell from the two opposite sides, which strongly supports our XRD results that revealed complete nanowire straightening.

It is worth it to mention that the presence of misfit dislocations and defects has been reported by TEM for highly bent radial nanowire heterostructures with high lattice mismatch between the core and the shell(s) [37]. However, considering the unique elastic properties of nanowires, their ability to sustain strain more efficiently compared to planar systems, and that the nominal In concentration in the QW is only 8% (core–shell mismatch of around 0.57%), the formation of misfit dislocations during nanowire bending and straightening is not expected, and therefore similar TEM investigation as in [37] was not required.

Furthermore, considering the complexity of precisely implementing the thickness and compositional inhomogeneities of the nanowire shell(s) displayed in figure 4(e) into the FEM model, shell growth on only one side of the core was considered. However, it must be addressed that if the thickness of the GaAs outer shell at the adjacent side facets of LP1 and LP2 is not identical, shear strain increase or torsion can take place. Moreover, (In,Ga)As shell growth at the side facets opposite to LP1 and LP2 can decreases the total axial strain. However, the (In,Ga)As shell at the opposite side facets to LP1 and LP2 is only 1.5–3 nm in thickness, and around 2% in composition which would result in negligible opposing strain. Furthermore, torsion can be neglected as the thickness difference of the GaAs outer shell at the adjacent side facets to LP1 and LP2 is very small.

GaAs/(In,Ga)As/GaAs radial nanowire heterostructures provide a promising path to produce light emitting diodes, solar cells, and transistors. However, surface states can reduce conductivity and optical emission due to Fermi level pinning and depletion of charge carriers, thus rendering them unusable for device structures. Therefore, surface passivation is crucial in order to enhance and explore the optical emission of these nanowire heterostructures. The most widely used GaAs nanowire surface passivation methods utilize closely lattice matched shells of a different material i.e. AlGaAs [38, 39], AlIn [40] or InGaP [41], or lattice mismatched ultrathin GaP and InP capping layers [42]. Passivation, for example, with a thick (Al,Ga)As shell is typically employed to suppress the surface recombination of photoexcited electrons and holes in order to enhance the photoluminescence intensity [43]. The (Al,Ga)As shell would then be capped with a thin GaAs shell to avoid oxidation of Al. Moreover, higher In concentration in the (In,Ga)As quantum well would facilitate distinguishing the quantum well emission from that of GaAs.

Surface passivation by one of the above-listed materials is out of scope for this work since growth in our pMBE chamber is limited to Ga, In and As only. Furthermore, the indium concentration, and thus core–shell lattice mismatch, was intentionally chosen low in order to insure a low retrievable bending, since the reported nanowire bending-straightening experiment was the first of its kind. However, structural parameters i.e. nanowire length, shell-to-core volume ratio, and material composition can impact the nanowire bending and straightening processes. The longer the nanowire is, the thicker the shell is, and/or the higher the indium concentration is, the more the nanowire bends. To find out the critical nanowire length, shell thickness, and indium concentration at which nanowire

straightening is no longer possible, dedicated *in situ* experiments would have to be conducted, which is also not in the scope of the present work. Moreover, the advantages provided by straight core–shell nanowires with inhomogeneous shell compared to straight core–shell nanowires with all-around homogeneous shell is still unclear, due to missing optical or electrical characterization of both nanowire systems. Nevertheless, our study lays out the growth scheme of this rather new nanowire system which can be replicated, modified, investigated, and further improved.

Acknowledgments

Data availability statement

All data that support the findings of this study are included within the article (and any supplementary files).

ORCID iDs

Ali Al Hassan ⬤ https://orcid.org/0000-0002-2924-4215

References

[1] Balaghi L *et al* 2021 High electron mobility in strained GaAs nanowires *Nat. Commun.* **12** 6642

[2] Dayeh S A, Soci C, Bao X-Y and Wang D 2009 Advances in the synthesis of InAs and GaAs nanowires for electronic application *Nano Today* **4** 347–35

[3] Bae M-H, Kim B-K, Ha D-H, Lee S J, Sharma R, Choi K J, Kim J-J, Choi W J and Shin J C 2014 Non-lithographic growth of core–shell GaAs nanowires on Si for optoelectronic applications *Cryst. Growth Des.* **14** 1510–5

[4] Yao M, Cong S, Arab S, Huang N, Povinelli M L, Cronin S B, Dapkus P D and Zhou C 2015 Tandem solar cells using GaAs nanowires on Si: design, fabrication, and observation of voltage addition *Nano Lett.* **15** 7217–24

[5] Wang W I 1984 Molecular beam epitaxial growth and material properties of GaAs and AlGaAs on Si (100) *Appl. Phys. Lett.* **44** 1149

[6] Yamaguchi M, Yamamoto A, Tachikawa M, Itoh Y and Sugo M 1988 Defect reduction effects in GaAs on Si substrates by thermal annealing *Appl. Phys. Lett.* **53** 2293–5

[7] Martensson T, Svensson C P T, Wacaser B A, Larsson M W, Seifert W, Deppert K, Gustafsson A, Wallenberg L R and Samuelson L 2004 Epitaxial III–V Nanowires on Silicon *Nano Lett.* **4** 1987–90

[8] Biermanns A, Breuer A, Trampert A, Davydok A, Geelhaar L and Pietsch U 2012 Strain accommodation in Ga-assisted GaAs nanowires grown on silicon (111) *Nanotechnology* **23** 305703

[9] Glas F 2015 Strain in nanowires and nanowire heterostructures *Semiconducters Semimetals* **93** 79–123

[10] Kavanagh K L 2010 Misfit dislocations in nanowire heterostructures *Semiconductor Sci. Technol.* **25** 024006

[11] Gronqvist J, Søndergaard N, Boxberg F, Guhr T, Åberg S and Xu H Q 2009 Strain in semiconductor core–shell nanowires *J. Appl. Phys.* **106** 053508

[12] Sekiguchi H, Kishino K and Kikuchi A 2008 GaN/AlGaN nanocolumn ultraviolet light-emitting diodes grown on n-(111) Si by RF-plasma-assisted molecular beam epitaxy *Electron. Lett.* **44** 151–2

[13] Svensson C P T, Mårtensson T, Trägårdh J, Larsson C, Rask M, Hessman D, Samuelson L and Ohlsson J 2008 Monolithic GaAs/InGaP nanowire light emitting diodes on silicon *Nanotechnology* **19** 305201

[14] Tomioka K, Motohisa J, Hara S, Hiruma K and Fukui T 2010 GaAs/AlGaAs core multishell nanowire-based light-emitting diodes on Si *Nano Lett.* **10** 1639–44

[15] Dimakis E, Jahn U, Ramsteiner M, Tahraoui A, Grandal J, Kong X, Marquardt O, Trampert A, Riechert H and Geelhaar L 2014 Coaxial multishell (In,Ga)As/GaAs nanowires for near-infrared emission on Si substrates *Nano Lett.* **14** 2604–9

[16] Lewis R B, Nicolai L, Küpers H, Ramsteiner M, Trampert A and Geelhaar L 2017 Anomalous strain relaxation in core–shell nanowire heterostructures via simultaneous coherent and incoherent growth *Nano Lett.* **17** 136–42

[17] Balaghi L, Bussone G, Grifone R, Hübner R, Grenzer K, Ghorbani-Asl M, Krasheninnikov A V, Schneider H, Helm M and Dimakis E 2019 Widely tunable GaAs bandgap via strain engineering in core/shell nanowires with large lattice mismatch *Nat. Commun.* **10** 2793

[18] Jacobsen R S *et al* 2006 Strained silicon as a new electro-optic material *Nature* **441** 199–202

[19] Nam D, Sukhdeo D S, Kang J H, Petykiewicz J, Lee J H, Jung W S, Vučković J, Brongersma M L and Saraswat K C 2013 Strain-induced pseudoheterostructure nanowires confining carriers at room temperature with nanoscale-tunable band profiles *Nano Lett.* **13** 3118–23

[20] McDermott S and Lewis R B 2021 Bending of GaAs-InP core–shell nanowires by asymmetric shell deposition: implications for sensors *ACS Appl. Nano Mater.* **4** 10164–72

[21] Lewis R B, Corfdir P, Küpers H, Flissikowski T, Brandt O and Geelhaar L 2018 Nanowires bending over backward from strain partitioning in asymmetric core–shell heterostructures *Nano Lett.* **18** 2343–50

[22] Al-Humaidi M *et al* 2022 *In situ* x-ray analysis of misfit strain and curvature of bent polytypic GaAs-InGaAs core–shell nanowires *Nanotechnology* **33** 015601

[23] Al-Humaidi M *et al* 2023 Exploiting flux shadowing for strain and bending engineering in core–shell nanowires *Nanoscale* **15** 2254–61

[24] Panciera F, Baraissov Z, Patriarche G, Dubrovskii V G, Glas F, Travers L, Mirsaidov U and Harmand J-C 2020 Phase selection in self-catalyzed GaAs nanowires *Nano Lett.* **20** 1669–75

[25] Jacobsson D, Panciera F, Tersoff J, Reuter M C, Lehmann S, Hofmann S, Dick K A and Ross F M 2016 Interface dynamics and crystal phase switching in GaAs nanowires *Nature* **531** 317–22

[26] AlHassan A, Salehi W A, Lewis R B, Anjum T, Sternemann C, Geelhaar L and Pietsch U 2021 Transition from elastic to plastic strain release in core–shell nanowires revealed by in-plane x-ray diffraction *Nanotechnology* **32** 205705

[27] AlHassan A *et al* 2020 Spatially-resolved luminescence and crystal structure of single core–shell nanowires measured in the as-grown geometry *Nanotechnology* **31** 214002

[28] Schroth P *et al* 2019 Impact of the shadowing effect on the crystal structure of patterned self-catalyzed GaAs nanowires *Nano Lett.* **19** 4263–71

[29] Slobodskyy T, Schroth P, Grigoriev D, Minkevich A A, Hu D Z, Schaadt D M and Baumbach T 2012 A portable molecular beam epitaxy system for *in situ* x-ray investigations at synchrotron beamlines *Rev. Sci. Instrum.* **83** 105112

[30] Tauchnitz T, Nurmamytov T, Hübner R, Engler M, Facsko S, Schneider H, Helm M and Dimakis E 2017 Decoupling the two roles of Ga droplets in the self-catalyzed growth of GaAs nanowires on SiO$_x$/Si (111) substrates *Cryst. Growth Des.* **17** 5276–82

[31] Jakob J, Schroth P, Feigl L, Al-Humaidi M, AlHassan A, Davtyan A, Hauck D, Pietsch U and Baumbach T 2021 Correlating *in situ* RHEED and XRD to study growth dynamics of polytypism in nanowires *Nanoscale* **13** 13095–107

[32] Pietsch U, Holy V and Baumbach T 2004 *High-Resolution X-ray Scattering: From Thin Films to Lateral Nanostructures* (Springer Science & Business Media)

[33] Nye J F 1985 *Physical Properties of Crystals: Their Representation by Tensors and Matrices* (Oxford University Press)

[34] Hearmon R F S 1961 *An Introduction to Applied Anisotropic Elasticity* (Oxford University Press)

[35] Wang S Q and Ye H Q 2003 First-principles study on elastic properties and phase stability of III–V compounds *Phys. Status Solidi Basic Res.* **240** 45–54

[36] Pan E 2002 Elastic and piezoelectric fields in substrates GaAs (001) and GaAs (111) due to a buried quantum dot *J. Appl. Phys.* **91** 6379–87

[37] Davtyan A *et al* 2020 X-ray diffraction reveals the amount of strain and homogeneity of extremely bent single nanowires *J. Appl. Cryst.* **53** 1310–20

[38] Chang C-C *et al* 2012 Electrical and optical characterization of surface passivation in GaAs nanowires *Nano Lett.* **12** 4484

[39] Dhaka V *et al* 2013 Aluminum-induced photoluminescence red shifts in core–shell GaAs/AlGaAs nanowires *Nano Lett.* **13** 3581

[40] Chia A C E, Tirado M, Li Y, Zhao S, Mi Z, Comedi D and LaPierre, R R 2012 Electrical transport and optical model of GaAs-AlInP core–shell nanowires *J. Appl. Phys.* **111** 094319

[41] Sköld N, Karlsson L S, Larsson M W, Pistol M-E, Seifert W, Trägårdh J and Samuelson L 2005 Growth and optical properties of strained GaAs-GaInP core–shell nanowires *Nano Lett.* **5** 1943

[42] Haggren T, Jiang H, Kakko J-P, Huhtio T, Dhaka V, Kauppinen E and Lipsanen H 2014 Stron surface passivation of GaAs nanowires with ultrathin InP and GaP capping layers *Appl. Phys. Lett.* **105** 033114

[43] Küpers H, Corfdir P, Lewis R B, Flissikowski T, Tahraoui A, Grahn H T, Brandt O and Geelhaar L 2019 Impact of outer shell structure and localization effects on charge carrier dynamics in GaAs/(In,Ga)As nanowire core–shell quantum wells *Physica Status Solidi (RRL)* **13** 1800527